Eur. Phys. J. B (2025) 98:47
https://doi.org/10.1140/epjb/s10051-025-00893-7

THE EUROPEAN PHYSICAL JOURNAL B

Regular Article - Computational Methods

Modulating the electronic and optical properties of $InGeF_3$ perovskite under pressure: a computational approach

Mohammed Miri[1,2,a], Younes Ziat[1,2], Hamza Belkhanchi[1,2], Ayoub Koufi[1,2], and Youssef Ait El Kadi[1]

[1] Laboratory of Engineering and Applied Physics Team (EAPT), Sultan Moulay Slimane University, Beni Mellal, Morocco
[2] The Moroccan Association of Sciences and Techniques for Sustainable Development (MASTSD), Beni Mellal, Morocco

Received 6 December 2024 / Accepted 23 February 2025 / Published online 18 March 2025

Abstract. This study explores the structural, mechanical, electronic and optical properties of $InGeF_3$ perovskite under varying pressures using density functional theory (DFT) via the Wien2k code. Elastic constants meet mechanical stability criteria at 0 GPa, with a notable improvement in ductility and hardness under pressure. Electronic analysis reveals an indirect band gap of 1.51 eV at 0 GPa, narrowing to 0.67 eV at 9 GPa, signaling a transition to metallic behavior. The density of states shows the dominance of halogens in the valence band, and significant contributions from indium and germanium in the conduction band. Optical properties, such as absorption and reflectivity, evolve under pressure, with a shift of the absorption spectrum toward lower energies. These findings demonstrate that pressure not only modifies the electronic structure of $InGeF_3$ but also enhances its optical performance, making it a potential candidate for photovoltaic applications.

1 Introduction

Growing energy consumption is encouraging the search for alternative, more efficient sources of production, such as solar and wind power [1–4]. Renewable energies based on solar cells are particularly important, both economically and environmentally [5–9]. These energies are clean, emit no polluting gasses and help preserve the environment [10]. The use of solar concentrators limits soil pollution, reducing its harmful effects and protecting public health. Due to the growing importance and wider use of solar cells [4, 11], researchers have developed techniques to improve their performance, notably by evaluating their electronic structure, using photovoltaic technologies, photoluminescence and light-emitting diodes (LEDs) [12, 13].

Solar cells are mainly made of perovskites, materials discovered by researchers John et al. [14]. Perovskites have an ABX_3-type crystal structure, where "A" and "B" are metal cations, "A" being larger than "B", and "X" is an anion, often an oxide or halogen, present in a cubic unit cell [15]. Identified as one of the most promising materials for power generation [16], perovskites are particularly prized in solar cells due to their excellent photoelectric properties [17–19]. Several researchers have studied these compounds using density functional theory (DFT), which enables quantum solids to be analyzed [20–23]. Perovskites are studied theoretically using generalized gradient approximation (GGA), GGA-modified Becke–Johnson (GGA-mBJ), GGA with spin–orbit coupling (GGA + SOC) and hybrid functional (HF) in the domain of density functional theory (DFT) [24–26]. Notable among these is the study of the compound $CsXCl_3$ (X = Sn, Pb) by Idrissi et al. [27], which revealed that these materials exhibit both non-magnetic and semiconducting behavior. It was observed that the bandgap of photovoltaic perovskites varies as a function of lattice parameter "a_0" (Å), with an increase in bandgap as the lattice parameter increases for $CsSnCl_3$ and $CsPbCl_3$ materials, which the band gap is the energy difference between the valence band and the conduction band, determining a material's electronic and optical behavior. It is crucial for semiconductors, influencing their conductivity and applications in devices properties [19]. However, most of this work remains focused on exploring the fundamental properties of these materials.

Efforts are being made to develop and evaluate these compounds and increase their performance, by introducing a pressure mechanism as a tool to modify and improve these properties, and thus the materials will be made more suitable and efficient in solar cell applications [28]. In this context, several studies have evaluated the properties of the materials and developed

[a] e-mail: miri.estbm@gmail.com (corresponding author)

them, we mention the study of the compound $AGeF_3$ (A = K, Rb) by Md. Safin Alam et al. [29], who explore that decrease in the bond dimension and lattice parameters under pressure leads to increased interaction between atoms, which leads to increased bonding forces under pressure. Using hydrostatic pressure, significant changes in optical absorption and conductivity are also observed, as reduction of the band, which contributed to an enhanced conduction. Moreover, the study of $CsSnCl_3$ element by Md. Majibul et al. [30] also found that the electron density is affected by increasing the pressure of the states approaching the Fermi level. Thus, the absorption peak shifts toward lower photon energies, and hence the absorption coefficient is improved.

Indium-based perovskites, such as $InGeF_3$, are metal-halogen materials due to the presence of fluorine, a member of the halogen family. Although their structural and optoelectronic properties have been studied in general, there is as yet no in-depth research into the modification or doping of these materials. This motivates us to study the effect of pressure to better understand their behavior and optimize their performance. In this work, we aim to carry out a comprehensive analysis of the optoelectronic and elastic properties of $InGeF_3$ perovskites, using density functional theory (DFT), a computational method recognized for its accuracy and efficiency in predicting material properties. The application of pressure makes it possible to study the evolution of optoelectronic and elastic properties as a function of induced structural modifications. In this study, pressures ranging from 0 to 9 GPa will be applied. Under the influence of pressure, interatomic distances, bond angles and crystalline symmetry are modified, thus affecting material properties [31].

2 Calculation methodology

The method used to calculate the properties of the $InGeF_3$ material is the density functional theory (DFT), applied in the WIEN2k code [32–37]. The generalized gradient approximation (GGA-PBE) [38] was employed to evaluate the optoelectronic structural characteristics. The GGA method is utilized to assess the exchange and correlation elements [39]. In the context of GGA [40], the cross-correlation energy of a unit volume is not only related to the density within this volume but also to the densities in adjacent volumes. WIEN2K allows approximations in the description of electron density according to the GGA scheme, in organizing the electron space and the fundamental electron function model (APW). These approximations strike a balance between accuracy and computational efficiency. The model is based on the APW, which divides space into an internal region within the atomic sphere and an external region where a plane wave is used to describe electronic states. An approximation here is to limit the potential description to the interior of the atomic sphere, neglecting the long-range field effects outside, which might not fully account for long-range interactions between atoms. The GGA approach enhances the accuracy of calculations by considering electronic correlations. In DFT, the total energy of the system is used to compute the electron density, which describes the distribution of electrons in space. The GGA extends this by adding corrections to account for spatial fluctuations in electron density and density gradients. These energy calculations integrate such spatial fluctuations, improving the description of molecular systems. The GGA method primarily relies on integrating a function related to the density gradient, in addition to the electron density itself. WIEN2K employs a k-point mesh to integrate electronic properties in the reciprocal space. Static calculations are performed using 1000 k-points in the reciprocal space. This number is chosen based on the size of the primitive cell in real space and the required precision. The k-points are selected to ensure adequate precision in integrations, balancing computational load and result accuracy, while adhering to an energy convergence limit of 10^{-5} Ry. The atomic sphere radii (RMT) and the maximum modulus of the reciprocal vector are multiplied (Kmax = 7), ensuring a precise expansion of wave functions in plane wave series. The muffin tin radii (RMT) used are (2.50, 2.50, 2.32). Multiplying these parameters (RMT, Kmax) ensures that the plane waves used in describing electronic states are sufficiently accurate near the nuclei, while optimizing the number of reciprocal vectors in regions where plane waves are most appropriate. This method determines the cutoff for reciprocal vector expansion, ensuring high accuracy while minimizing the number of vectors needed.

3 Results and discussion

3.1 Structural properties

The crystalline unit cell of $InGeF_3$ is a cubic structure belonging to the family of simple inorganic metal halide perovskites, it is visualized in Fig. 1, which represents the structures of these elements that contain five atoms in each unit cell. These materials have a cubic structure that is part of space group #221 ($Pm\bar{3}m$) where the In cation is located at coordinates (0, 0, 0) and the Ge metal atom takes position (0.5, 0.5, 0.5), while the F anion is located at coordinates (0.5, 0, 0.5), (0.5, 0.5, 0) and (0, 0.5, 0.5) in Wyckoff coordinates [41].

Optimization of the lattice parameters is a process that stabilizes the overall system, and lies in the microscopic adjustment of the cell size of the nanomaterials studied, and their volume is related to the total energy E. From the regression of volume values against pressure, which are represented by Murnaghan's equation [42], we can find the minimum energy E_0 to which the volume V_0 corresponds. These are two modules that can be extracted from the values of the compressibility coefficient B and its derivative B', using

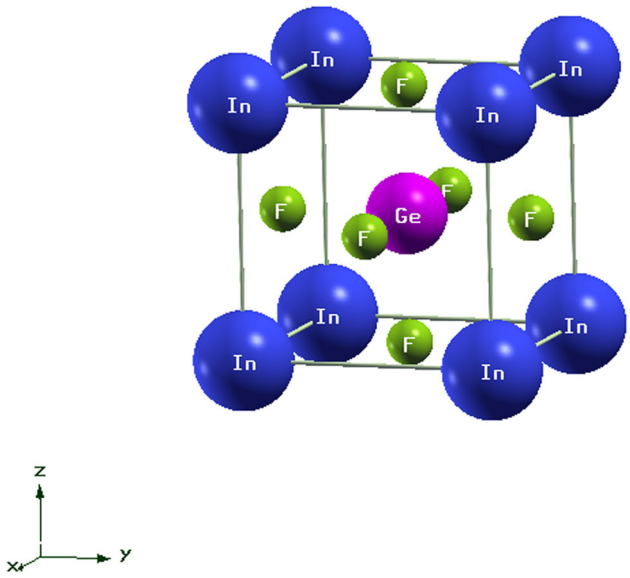

Fig. 1 Structure of crystalline $InGeF_3$

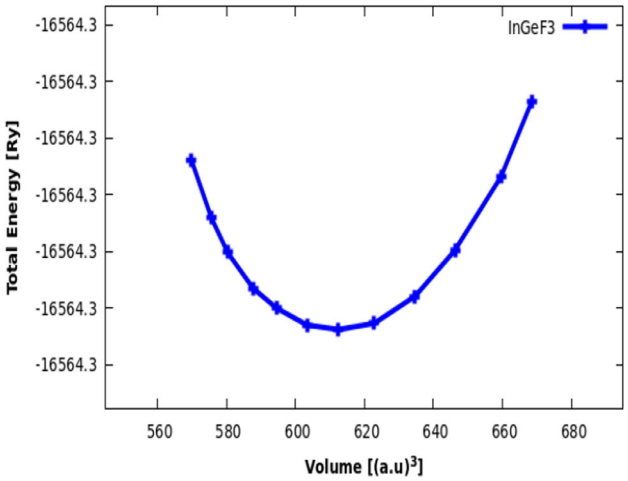

Fig. 2 Variation of total energy as a function of volume for $InGeF_3$

Birch–Mornaghan's Eq. (1) (EOS) [43], these values are presented in Table 1.

$$E = E_0 + \frac{B_0}{B_0'}(V - V_0) - \frac{B_0 V_0}{B_0'(1 - B_0')}\left[\left(\frac{V}{V_0}\right)^{1-B_0'} - 1\right] \quad (1)$$

This method consists of reducing the total energy value E while optimizing the size of the cells to obtain two optimized parameters B and B' at zero pressure are illustrated in Fig. 2. As two parameters, the former contributes to the force amplification, while the latter contributes to recover the thermoplastic aspects and measures the crystal rigidity of the material [44]. Table 1 summarizes the values of the optimized parameters obtained E, V, B and B', during the optimization process.

Hydrostatic pressure strongly affects the structural properties and also directly changes the electronic properties of $InGeF_3$. As the pressure increases, in the range of 0–9 GPa, it remains to determine the specific pressure associated with the modification of the energy band of the material. In this study, we analyzed a change in the behavior of a semiconductor material, focusing on an exceptional pressure not exceeding 9 GPa. This restriction aims to gradually reduce the energy gap in order to preserve the semiconductor character of the material. The lattice constant gradually decreases, leading to a decrease in the cell volume, and this pressure brings the atoms closer together, thereby strengthening the chemical bonds. This phenomenon increases the interatomic forces, which increases the strength and hardness of the crystals. In addition, the increased overlap of atomic orbitals under pressure reduces the energy gap between the valence band and the conduction band, thereby reducing the band gap width. This research on the effect of the parameters and the gap energy as a function of pressure is consistent with the results of other studies reported in the literature [46]. Table 2 shows the variation of the lattice parameters and the band energy as a function of pressure. These improvements expand the potential applications of $InGeF_3$ in demanding industries, such as aerospace, petrochemicals or advanced devices based on this technology.

To analyze the stability of crystal structures and the distortions that can occur, we use the Goldschmidt tolerance factor, a key tool in crystallography [47]. This factor is used to assess the effects of size differences between the cations present in the crystal lattice. More precisely, it estimates the geometric compatibility between the constituent ions and their arrangement in the crystal structure. The tolerance factor is calculated from the ionic radii R_{In}, R_{Ge}andR_F, which respectively represent the radii of atoms A, B and F

Table 1 Calculated optimized parameters a_0, V, E, B and B', τ_G and ΔH_f of $InGeF_3$

Parameter	Lattice parameter a_0 (Å)		Volume minimum V ([a.u]^3)	Energy minimum E (Ry)	Bulk modulus B (GPa)	Pressure derivative B'	Goldschmidt tolerance factor τ_G	Formation energy ΔH_f eV/atom
	Optimized	Ohter work						
Values	4.48	4.47 [45]	614.0330	− 16,564.3168	55.9494	5.2012	0.93	− 2.1

Table 2 Lattice parameter and gap energy of $InGeF_3$

Pressure GPa	Lattice parameter a_0 (Å)	Gap energy (eV)
0	4.48	1.51
3	4.39	1.19
6	4.32	0.91
9	4.26	0.67

in the crystal lattice, according to the following expression:

$$\tau_G = \frac{R_A + R_F}{\sqrt{2}(R_b + R_F)} \tag{2}$$

For perovskites, an ideal cubic structure is associated with a τ_G value between 0.75 and 1. A value close to 1 is indicative of a stable, symmetrical cubic structure. In the case of $InGeF_3$, the estimated value of τ_G is 0.93, as shown in the data (Table 1). This suggests that this compound possesses a stable structure close to the cubic ideal, characterized by relatively high symmetry and good geometric compatibility of cations and anions in the lattice.

In parallel, the thermodynamic stability of the compound is studied using its formation energy ΔH_f [48–50]. This parameter verifies whether the formation of the compound from its constituent elements in their standard state is thermodynamically favorable. The energy of formation corresponds to the change in energy involved when the elements react to form the compound. A negative value of ΔH_f indicates that the process is exothermic, i.e., it releases energy, reflecting an increased stability of the compound relative to its initial reactants. In other words, a compound with a negative formation energy is thermodynamically stable as it is in a lower energy state than its constituents [51–53].

The expression for the energy of formation is given by [54]:

$$\Delta H_f = E_{\text{tot}} - \mu_A - \mu_B - 3\mu_X, \tag{3}$$

where E_{tot} represents the total energy of the $InGeF_3$ compound, and μ_{Ge}, are the chemical potentials of the elements In, Ge and F respectively. According to the results presented in the Table 1, $InGeF_3$ has a negative energy of formation, providing strong evidence of its thermodynamic stability. This stability, combined with the favorable value of the tolerance factor, confirms that $InGeF_3$ is a stable crystalline compound, suitable for potential applications requiring robust perovskite structures.

3.2 Mechanical properties

Elastic constants of solids are parameters that describe the behaviors of mechanical properties. Cubic crystals such as the studied sample $InGeF_3$ are distinguished by three independent elastic constants Cij: (C_{11}, C_{12} and C_{44}) [55]. These coefficients can be used to identify the internal forces present in solid materials as well as their mechanical stability, and also they clarify and determine the relationship between the mechanical and dynamic properties of crystals [56]. To achieve mechanical stability of materials, elastic coefficients must meet the Born criteria given by [57].

$$\mathbf{C_{11} + 2C_{12} > 0},\ \mathbf{C_{11} - C_{12} > 0},\ \mathbf{C_{11} > 0 \text{ and } C_{11} > B > C_{12}}. \tag{4}$$

Analysis of Table 3 clearly shows the crystalline stability of $InGeF_3$ since the three elastic constants C_{11}, C_{12} and C_{44} satisfy the mechanical stability criteria, thus confirming the stability of the material studied. The values of the elastic constants at zero pressure are in agreement with previous theoretical results [45]. Here, we focus on the analysis of mechanical properties at applied pressures ranging from 0 to 9 GPa. The study reveals that mechanical constants increase progressively with increasing pressure, indicating that pressure enhances the ductility of the material. Observing the variations in coefficients under pressure, it appears that C_{11} and C_{12} increase rapidly compared to C_{44}. This increase in C_{11} and C_{12} is due to elastic length reinforcement under hydrostatic pressure, while C_{44}, which is related to shape flexibility, regulates the relationship between deformation and sample shape [58].

Cauchy pressure, defined as $Cp = C_{12}–C_{44}$ [59], is used to assess the brittleness and ductility of materials. This parameter is widely used to analyze soft and brittle materials. A negative Cauchy pressure indicates brittleness, while a positive pressure reflects ductility (see Table 3). In the case of $InGeF_3$ perovskite, Cauchy pressure remains positive for all pressures studied, and its values increase with increasing pressure. This suggests that the hardness of perovskite improves with pressure, enhancing its mechanical performance.

The mechanical properties of a material and the nature of its stiffness are assessed through the study of its elastic parameters, namely the shear modulus G, bulk modulus B, and Young's modulus E. These parameters are fundamental in describing the relationship between the forces applied to solid materials and their resulting deformations [38]. Using the calculated elastic constants (C_{ij}), these moduli are derived through established mathematical expressions. The calculations are based on the Voigt–Reuss–Hill approximation represented by the following formulas [60–64]:

$$B = \frac{C_{11} + 2C_{12}}{3}, \tag{5}$$

$$G = \frac{G_V + G_R}{2}, \tag{6}$$

$$E = \frac{9BG}{3B + G}, \tag{7}$$

Table 3 Calculated elastic constants C_{ij} of $InGeF_3$

Elastic coefficients C_{ij}	C_{11}	C_{12}	C_{44}	C_p
Pressure 0 GPa	93.21	44,87	22.91	21.96
Pressure 3 GPa	138.54	57.33	25.58	31.75
Pressure 6 GPa	175.76	70.73	28.61	42.12
Pressure 9 GPa	199.64	82.14	31.33	50.81

$$\nu = \frac{(3B - 2G)}{3(2B + G)}, \tag{8}$$

$$G_V = \frac{C_{11} - 2C_{12} + 3C_{44}}{5}, \tag{9}$$

$$G_R = \frac{5(C_{11} - C_{12})C_{44}}{4C_{44}+3(C_{11} - C_{12})}. \tag{10}$$

From the data in the Table 4, it can be seen that the parameters B, G, and E are sensitive to the effect of pressure. As the pressure increases from 0 to 9 GPa, the strength properties of the material change significantly. The bulk modulus (B) and the shear modulus (G) increase from 60.23 GPa and 23.40 GPa to 121.31 GPa and 40.37 GPa, respectively, indicating improved compressive strength under high pressure and "increased shear toughness." Similarly, the elastic modulus (E) increases from 62.23 GPa to 109.02 GPa for pressures from 0 to 9 GPa, indicating an overall improvement in the elastic properties of the material. It has also been reported in other works [45], which explore the fact that the parameters B, G and E in the absence of pressure have values of 58.94, 13.67 and 36.87, respectively. Based on the moduli B, G and E, two ratios can be determined: Pugh (B/G) [65], and Poisson's ratio (ν), both considered as criteria that describe the proposed mechanical behavior of crystals. B/G and v are identified the brittleness and toughness of materials according to their critical values 1.75, and 0.26 [66], respectively, whereas brittleness is indicated by a low value, ductility is linked to a high B/G ratio. Roughly 1.75 is the crucial number that divides materials into ductile and brittle categories; that is, (brittle $<$ 1.75 $<$ ductile) [60]. In addition, when Poisson's ratio is greater than 0.26, the material is ductile, and a larger value corresponds to a higher ductility [66]. The B/G ratio, which increases from 2.60 to 3.00 at a pressure of 9 GPa, indicates the tendency of the material to become softer with increasing pressure. The Poisson's ratio (ν) also increases from 0.311 to 0.334, still at pressure 0 to 9 GPa, reflecting an increased capacity to resist volumetric deformations and a more elastic behavior under high pressure. All these parameters show that the application of pressure improves the hardness and elastic properties of the material.

3.3 Electronic properties

The electronic properties are affected by the structural modification of crystalline due to impact of P, where the impact of P on parameter dimensions and cell size. The investigation of electronic structures allows the analysis of the distribution of valence and conduction bands, as well as the position of the Fermi level, and the different electronic states of solids (insulator, conductor, semiconductor, semimetal and half-metal) can also be distinguished [59]. The band structure of $InGeF_3$ perovskite was analyzed at pressures ranging from 0 to 9 GPa. At 0 GPa pressure, the band gap energy of $InGeF_3$ consists of an average value of 1.51 eV, indicating that it is a semiconductor material, and it is observed at the symmetry points "L" and "W" of the barylon region, indicating that this crystal gap is indirect, these results are in agreement with other studies [45], as shown in Fig. 3a. It should be emphasized that when increasing the pressure at 3, 6 and 9 GPa, the minimum value of CB shifts to level E_F, while the maximum value of VB shifts to lower energies, to the L symmetry point. Thus, the band gap maintains its nature of optical gap indirect (L–W), as shown by the calculated band gap values of 1.19 eV and 0.91 eV and 0.67 eV at 3 GPa, 6 GPa and 9 GPa, respectively. It can be concluded that the increase in pressure leads to a decrease in the atomic spacing and an increase in the interaction potential between the electron and the ion [67]. Reducing the lattice parameter, which reflects a decrease in the distance between atoms, results in a decrease in the band gap width, which enhances the difficult of electronic transfer between the valence band and conduction band near the Fermi level [68, 69]

Densities of electronic states, both total density (TDOS) and partial density (PDOS) provide a detailed analysis of the electronic components of $InGeF_3$ perovskite, allowing us to assess atomic hybridization and the contribution of each atom to the overall electronic configuration of the system. As shown in Figs. 4 and 5, the valence band is dominated by halogen atoms F, while metal atoms In and Ge contribute mainly to the conduction band, with a preponderance of In-d and Ge-p orbitals. F-p orbitals largely define the valence band, particularly between − 6 and − 4 eV, underlining the importance of fluorine in electronic properties and chemical bonding, while In-d and Ge-p orbitals play a key role in the conduction band, particularly between 2 and 4 eV. Under pressure, the peaks of the Ge-p and F-p orbitals in the conduction band approach and converge around the Fermi level (E_F), while the p orbitals of F in the valence band shift to lower energies, from − 3.5 eV and − 4.5 eV to around − 4 eV and − 6.1 eV under increased pressure (up to 9 GPa). These shifts are attributed to the reduction in interatomic distance and

Table 4 Calculated elastic modulus B, G, E, (B/G) et v of $InGeF_3$

Pressure (GPa)	B	G	E	B/G	v
0	60.98	23.40	62.23	2.60	0.311
3	84.40	30.81	82.40	2.75	0.320
6	105.74	36.57	98.37	2.89	0.328
9	121.31	40.37	109.02	3.00	0.334

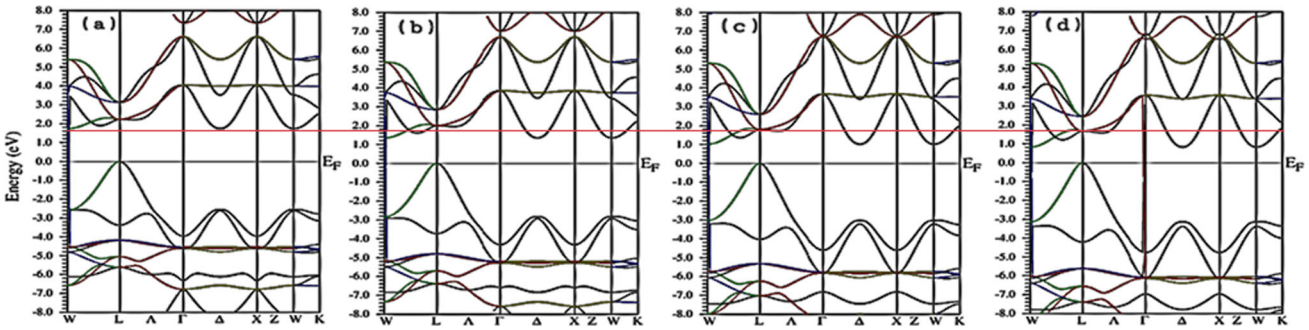

Fig. 3 Band structure of $InGeF_3$ at **a** 0 GPa, **b** 3 GPa, **c** 6 GPa and **d** 9 GPa

the modification of interaction potentials under pressure, leading to a transition of the material from a semiconductor to a metal-like structure [70]. To extend this analysis, we have examined the distribution of electronic charge density to visualize changes in chemical bonds under pressure. By studying charge density and projected densities of states (PDOS), we can observe how pressure modifies orbital interactions and strengthens certain bonds. In particular, the redistribution of charge density indicates an increase in hybridization between the orbitals of In, Ge and F atoms, highlighting a strengthened electronic interaction under pressure. This result confirms that the simple reduction in interatomic distance is not sufficient to explain bond strengthening, but that a tuning of electronic interactions and orbital coupling effects must be taken into account, as mentioned in the literature [46, 71, 72]. Other studies show that pressure can induce important structural and electronic transitions, transforming semiconducting materials from a semiconducting phase to one with metallic properties [45, 70, 73]. This process, known as pressure-induced metallic transition, reveals how external mechanical stresses can be used to alter the electronic nature of a material and make it more conductive. This opens up new prospects for the development of adaptive electronic and optoelectronic devices, where material properties can be dynamically controlled by pressure.

3.4 Optical properties

Using the DFT method, we were able to study the effect of pressure on the optical properties of the material in detail, including examining changes in the absorption spectrum. Under pressure, the crystal structure is distorted, and thus the configuration of the electronic bands changes. These changes directly affect how the material interacts with light, changing the absorption energy and intensity at different wavelengths. DFT allows us to track these changes precisely and analyze how the electronic transitions are affected by pressure. In short, this approach provides us with a deep understanding of the relationship between applied pressure, electronic structure, and optical properties. Using WIEN2k to calculate the optical properties, the calculations were carried out under the generalized gradient approximation (GGA) with the Perdew–Burke–Ernzerhof (PBE) functional to account for the exchange–correlation interactions. These approximations are commonly used for the calculation of the electronic structure and optical properties, ensuring a reasonable balance between computational efficiency and accuracy.

According to the values of the band gaps of the elements studied in the ultraviolet and visible range, then these materials seem suitable for optoelectronic applications. However, there is more interest in improving and developing the performance of photovoltaic cells and solar panels. Hydrostatic pressure effect is found as a simple and effective way to modify the electronic structures to obtain the best optical properties. We studied $InGeF_3$ materials under induced pressure ranging from 0 to 9GPa, pressure modification is a very important procedure to evaluate different optical properties, such as absorption (a), optical conductivity, reflectivity (R), and refractive index (n), are parameters determined by the complex $\varepsilon(\omega)$ is a complex permittivity function that can be expressed as $\varepsilon(\omega) = \varepsilon_1(\omega) + i\varepsilon_2(\omega)$ [74], with ε_1 and ε_2 both can be calculated by the Kramers–Kronig equations [75, 76].

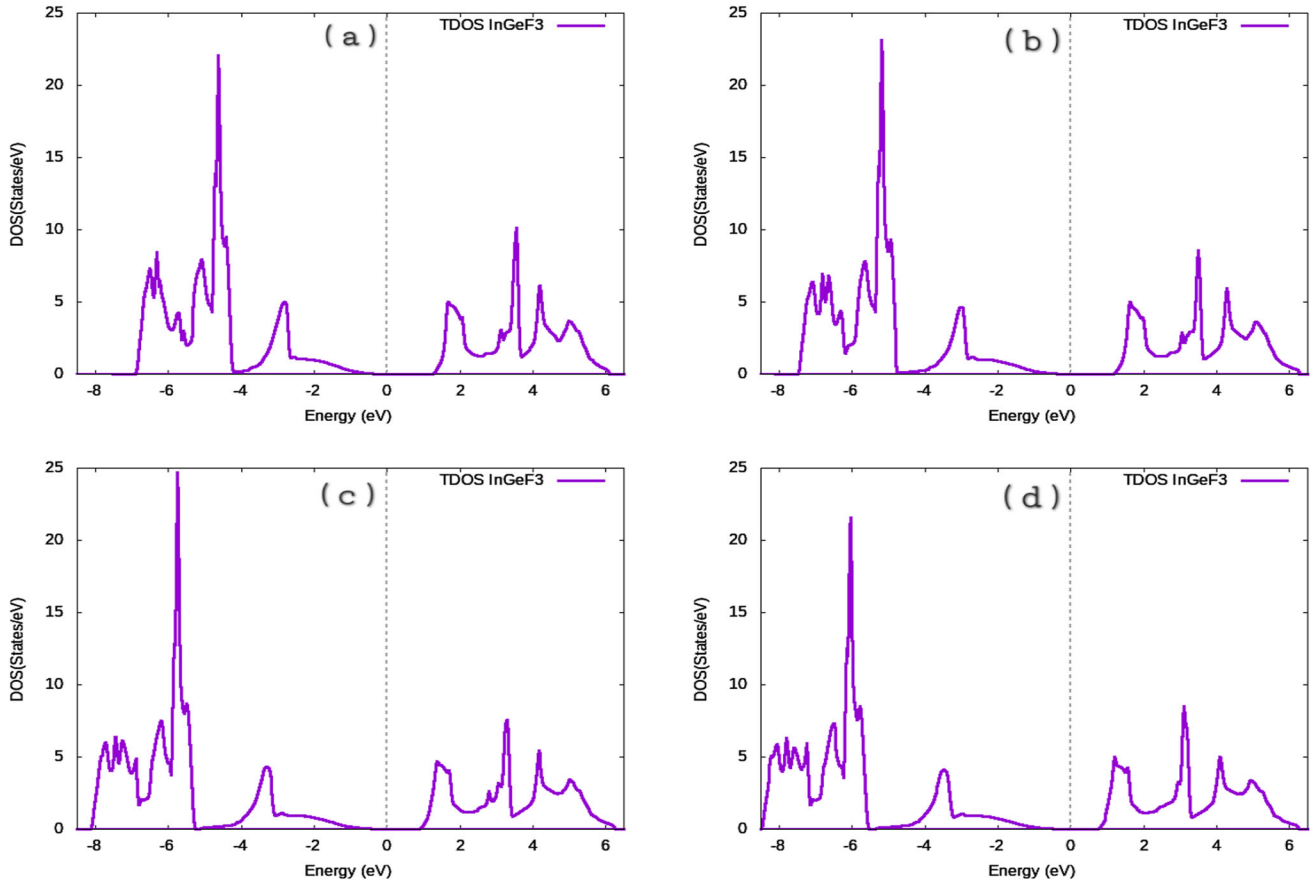

Fig. 4 TDOS of $InGeF_3$ at **a** 0 GPa, **b** 3 GPa, **c** 6 GPa and **d** 9 GPa

$$\varepsilon_1(\omega) = 1 + \frac{2}{\pi} p \int_0^{\infty} \omega' \varepsilon_2(\omega') \frac{d\omega'}{\omega'^2 - \omega^2}, \tag{11}$$

$$\varepsilon_2(\omega) = \left(\frac{4\pi^2 e^2}{\omega^2 m^2}\right) \sum_{i,j} < i|M|j >^2 f_i(1 - f_j)\delta(E_{j,k} - E_{i,k} - \omega) d^3k. \tag{12}$$

Based on the complex permittivity function, the absorption coefficient $\alpha(\omega)$, the reflectance $R(\omega)$, the complex refractive index $n(\omega)$, the extinction coefficient $\kappa(\omega)$ and the optical conductivity $\sigma(\omega)$ of the material can be determined using expressions [77, 78]:

$$\sigma(\omega) = \frac{\omega}{4\pi} \varepsilon_2(\omega), \tag{13}$$

$$\alpha(\omega) = \sqrt{2}\omega \left[\sqrt{\varepsilon_1^2(\omega) + \varepsilon_2^2(\omega)} - \varepsilon_1(\omega)\right]^{\frac{1}{2}}, \tag{14}$$

$$R(\omega) = \left|\frac{\sqrt{\epsilon(\omega)} - 1}{\sqrt{\epsilon(\omega)} + 1}\right|^2, \tag{15}$$

$$n(\omega) = \frac{1}{\sqrt{2}} \left[\sqrt{\varepsilon_1^2(\omega) + \varepsilon_2^2(\omega)} + \varepsilon_1(\omega)\right]^{\frac{1}{2}}. \tag{16}$$

From Fig. 6a, it is clear that at 0 eV the spectra of $\varepsilon 1(0)$ for crystalline $InGeF_3$ have the estimated values of 4.40, 4.80, 5.10 and 5.30 at pressures 0, 3, 6 and 9 GPa. The variation of $\varepsilon 1(\omega)$ with photon energy explores a progression until reaching the value of 6.20, 6.90, 7.50 and 8.00 under pressures 0, 3, 6 and 9 GPa respectively, corresponding to energy 2 eV, after this energy, the coefficient experiences a sharp decrease of value 4.50 at the different pressures studied 0 to 9GPa, corresponding to energy 4 eV, indicating the presence of a plasma resonance. After that, $\varepsilon 1$ (ω) slowly decreases and it approaches its minimum values in the energy range of 4.5–12 eV.

Figure 6b shows the part of the imaginary calculus $\varepsilon 2$ (ω) in the photonic energy function, illustrating this with the absorption of the light and the transitions inside the bands, telling you what the transition of the valence band is conduction band [79]. The first point of analysis occurs at 0 eV under 0 GPa, where the optimal transition direction corresponds to the maximum of the VB) and the minimum of the CB. Due to the reduction in the band gap, the fundamental absorption edge shifts to a higher energy region as pressure increases. Notably, the extent of this shift correlates with the magnitude of the band gap reduction. As pressure rises, the imaginary part of the $\varepsilon 2(\omega)$ exhibits three prominent peaks at approximately 3.10, 6.80, and 6.50,

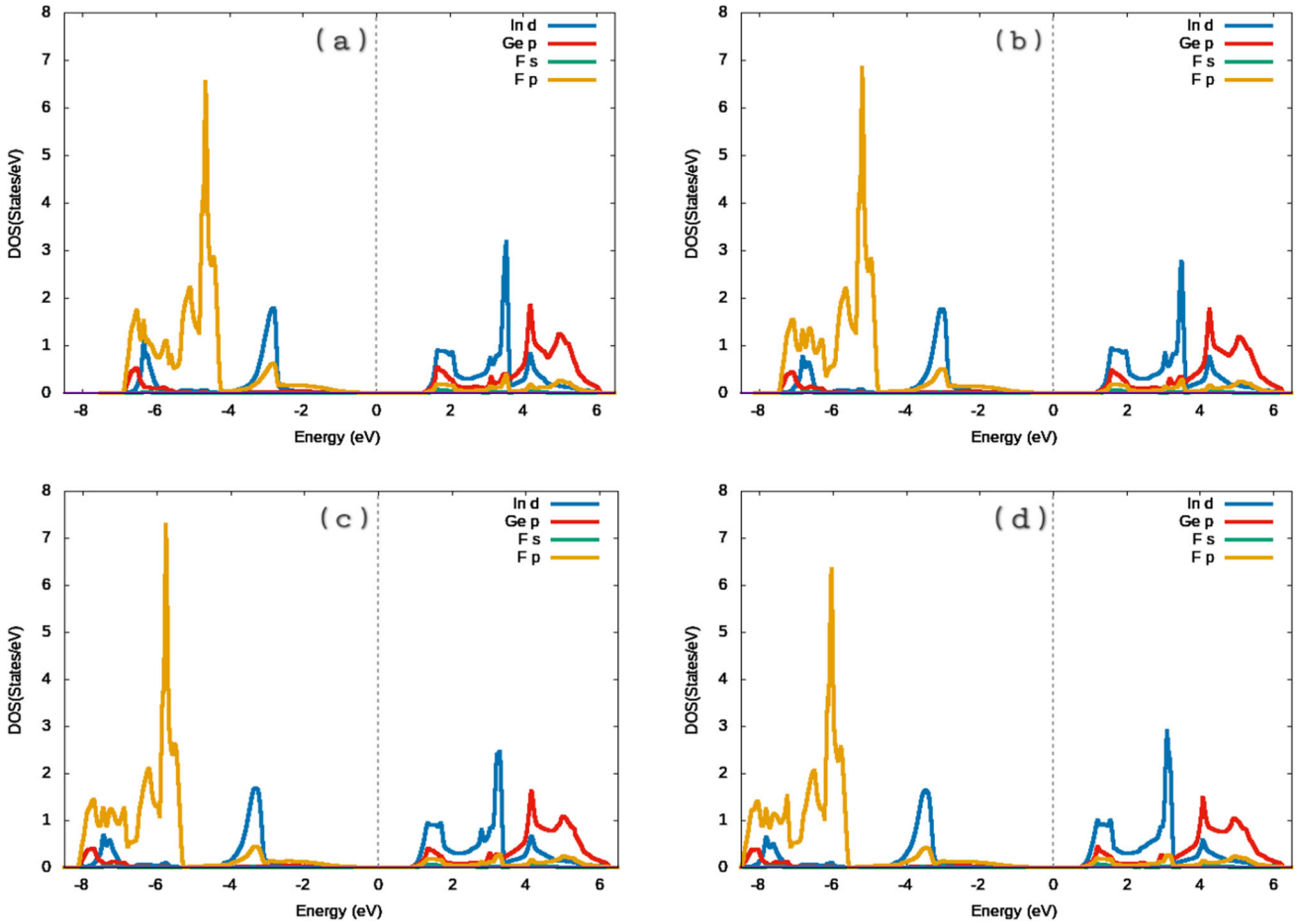

Fig. 5 PDOS of $InGeF_3$ at **a** 0 GPa, **b** 3 GPa, **c** 6 GPa and **d** 9GPa

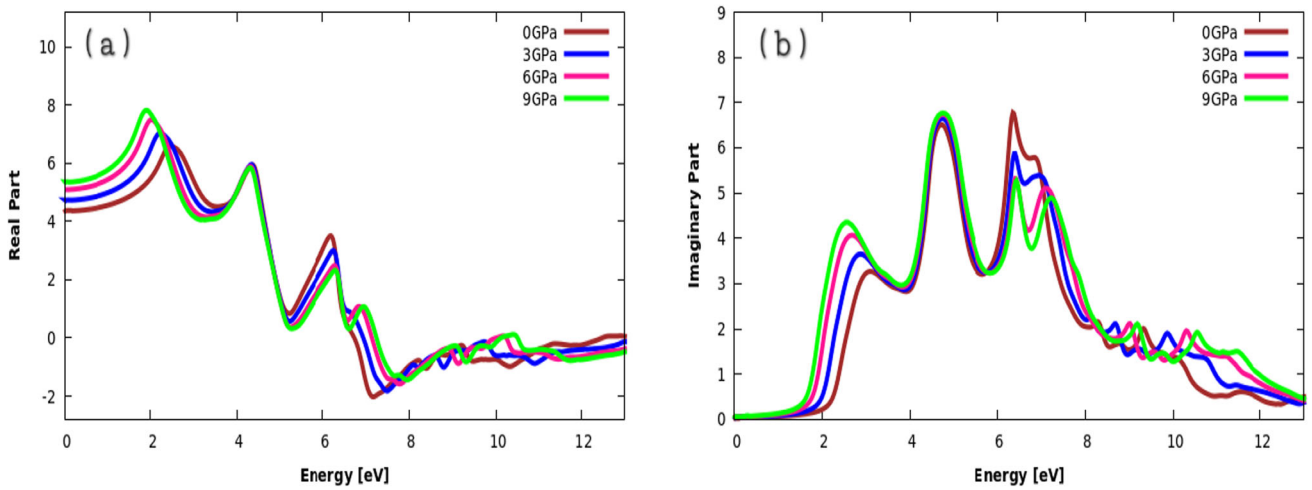

Fig. 6 **a** Real part and **b** imaginary part corresponding to the energy under pressure 0 GPa, 3 GPa, 6 GPa and 9 GPa of $InGeF_3$

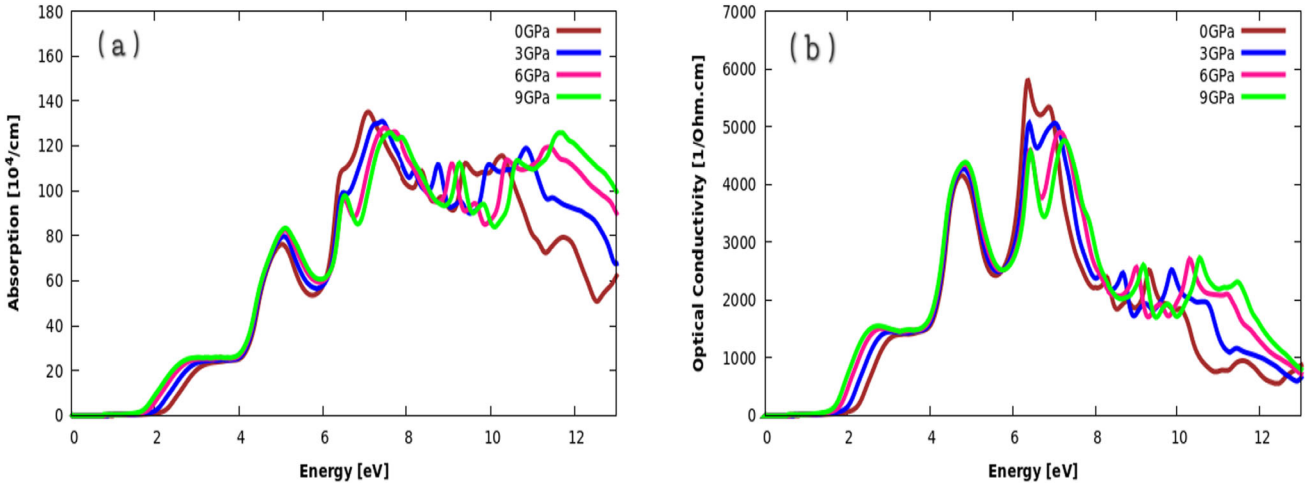

Fig. 7 **a** Absorption coefficient and **b** Conductivity versus energy under pressure 0 GPa, 3 GPa, 6 GPa and 9 GPa GPa of $InGeF_3$

corresponding to photon energies of 2.50 eV, 4.50 eV, and 6.40 eV, respectively. These peaks align with the main absorption features observed in the absorption spectrum. Specifically, the peak at 2.50 eV increases in intensity with pressure, reaching values of 3.60, 4.00, and 4.20 at pressures of 3 GPa, 6 GPa, and 9 GPa, respectively.

The absorption coefficient $\alpha(\omega)$ represents the rate of attenuation of light intensity per unit distance traveled in the material [80]. Figure 7a shows that the absorption spectrum of $InGeF_3$ is zero until energies reach values of around 2.10, 2.00, 1.90 and 1.80 eV at pressures of 0 GPa, 3 GPa, 6 GPa and 9 GPa respectively. Thereafter, the absorption coefficient increases progressively with energy, reaching maximum peaks of 75.00, 79.00, 82.00 and 84.50 at the respective pressures, around an energy of 5 eV. Notably, the value obtained under zero pressure aligns with results from previous studies reported in the literature [45, 73]. After reaching these peaks, the spectra decrease before rising rapidly with increasing energy to around 7.50 eV. Above this energy, the spectra remain virtually stable. We also note that the spectra are shifted toward the low-energy region as the pressure increases, indicating that the pressure applied to the $InGeF_3$ crystal significantly enhances its absorption in the visible and ultraviolet regions.

The optical conductivity (σ) of $InGeF_3$ under pressure, as illustrated in Fig. 7b, demonstrates a behavior similar to that of the absorption coefficient ($\alpha\backslash$). The spectrum of σ shifts toward lower energy values under pressure, accompanied by an increase in intensity as pressure rises. This behavior can be attributed to the generation of free charge carriers when the $InGeF_3$ crystal absorbs photons, thereby enhancing conductivity. Under pressure, the energy of the band gap decreases, facilitating the excitation of electrons and promoting electronic conduction. The increased pressure also intensifies orbital interactions and photon absorption, further improving the optoelectronic properties of the material. This enhanced conductivity and absorption relationship highlight the critical influence of external constraints, such as pressure, on tailoring the electronic and optical characteristics of $InGeF_3$. These findings are consistent with results reported in the literature [71], emphasizing the potential of pressure as a tool for optimizing materials like $InGeF_3$ for advanced technological applications involving electronic conduction and energy transfer.

Figure 8a shows the reflectivity spectra of $InGeF_3$ under different pressures. Reflectivity $R(\omega)$ represents the electronic interaction between reflected and incident light energy at the surface of crystalline materials [81]. It can be used to analyze optical transitions and the nature of a material's surface in the face of penetrating radiation. $R(0)$ reflectivity values for $InGeF_3$ are estimated at 0.130, 0.140, 0.155 and 0.160 at pressures of 0 GPa, 3 GPa, 6 GPa and 9 GPa respectively. This increase could be explained by structural and electronic modifications of the element under the effect of successive compressions. Thereafter, $R(\omega)$ increases progressively with photon energy until it reaches around 2.5 eV. After this threshold, reflectivity decreases rapidly to 4.0 eV. However, after this decrease, $R(w)$ shows a trend reversal, increasing again with increasing photon energy. These variations probably reflect material-specific electronic transitions, influenced by its absorption spectrum and intrinsic optical properties.

Spectral refraction (n), on the other hand, evaluates the transparency of the material with respect to radiation. From Fig. 8b. It has been observed that between 0 and 2.5 eV, the value of n (0) important for the case of 9GPa compared to the value of 6GPa and more important than 3 and 0 GPa which has the values 2.08, 2.18, 2.22, 2.27 and 2.33 for 0GPa 3GPa, 6GPa and 9GPa respectively. Moreover, this continuous change increases with increasing energy until reaching maximum values, where the values for the higher pressure are always the maximum values relative to the gradually lower pressure, and these correspond to energy values of 2 eV,

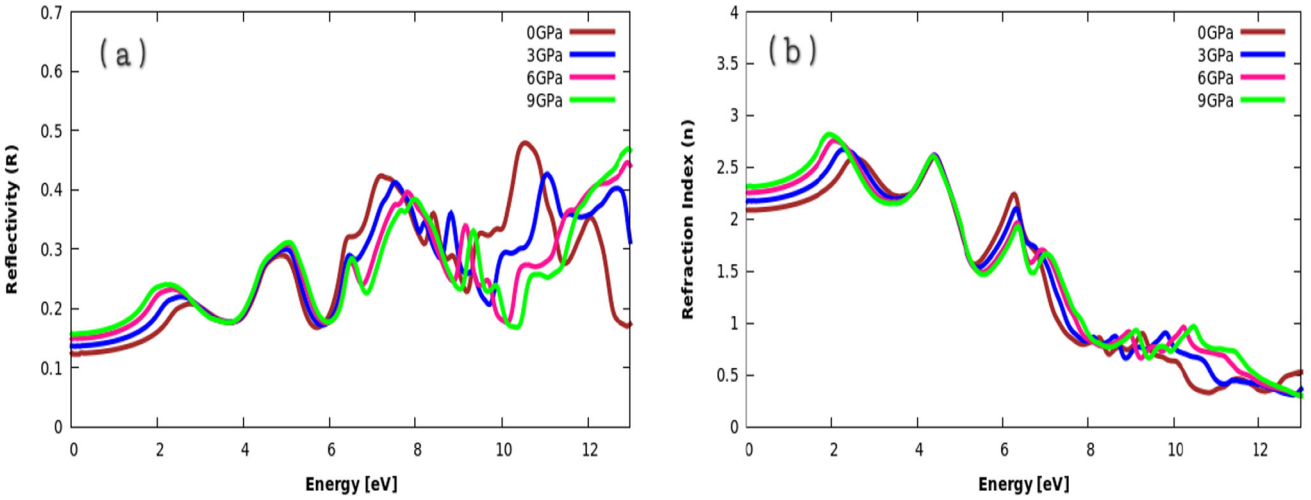

Fig. 8 **a** Reflectivity. **b** Reflective index corresponding to the energy under pressure 0 GPa, 3 GPa, 6 GPa and 9 GPa of $InGeF_3$

then n (ω) continues to decrease slowly up to the value of 0.75 corresponding to 12 eV. Literature studies, such as those on halide perovskites with similar optoelectronic characteristics, have shown that these properties strongly correlate with photovoltaic performance [82, 83].

4 Conclusion

The comprehensive analysis of $InGeF_3$ perovskite under various pressures reveals crucial insights into its mechanical, electronic, and optical behaviors. The elastic constants confirm the mechanical stability of the material, with increasing pressure enhancing its ductility and hardness. The narrowing of the bandgap with pressure indicates a gradual shift from semiconducting to metallic behavior, a trend supported by the DOS analysis and the band structure evolution. The impact of pressure on the optical properties is profound as the absorption and optical conductivity spectra shift toward lower energy, indicating enhanced performance in visible and ultraviolet regions. These improvements make $InGeF_3$ a promising material for photovoltaic and optoelectronic applications under high-pressure conditions. Future studies could explore other perovskite materials under varying pressures to further optimize their electronic and optical properties for energy-related technologies.

Acknowledgements The authors are warmly grateful to the support of "*The Moroccan Association of Sciences and Techniques for Sustainable Development (MASTSD), Beni Mellal, Morocco*," and to its president, professor *Charaf Laghlimi*, for the valuable proposals.

Author contributions

Mohammed Miri: writing the original draft, analyzing data, calculations, and validation. Younes Ziat: supervising. Hamza Belkhanchi: supervising and analyzing and validation. Ayoub Koufi; calculations. Youssef Ait El Kadi: validation. All authors read and approved the final manuscript. All authors contributed equally to the paper.

Data availability statement This manuscript has associated data in a data repository. [Author's comment: The data used in this study are original and obtained through our research work. All presented results are based on data collected and analyzed by the authors, and they are available upon request from the corresponding author.]

Declarations

Conflict of interest The authors have no conflicts of interest to declare. All co-authors have seen and agree with the contents of the manuscript, and there is no financial interest to report.

References

1. V. Nitsenko, A. Mardani, J. Streimikis, I. Shkrabak, I. Klopov, O. Novomlynets, O. Podolska, Crite-ria for evaluation of efficiency of energy transformation based on renewable energy sources. Montenegrin J. Econ. **14**(4), 237–247 (2018)
2. Y.F. Nassar, H.J. ElKhozondar, M.H. Abouqeelah, A.A. Abubaker, A.B. Miskeen, M.M. Khaleel et al., Simulating the energy, economic and environmental performance of concentrating solar power technologies using SAM: Libya as a case study. Solar Energy Sustain. Dev. **12**(2), 4–23 (2023). https://doi.org/10.51646/jsesd.v12i2.153

3. H. Korichi, A. Boucheham, A.B. Bensdira, M. Kazerane, Advancements in passivation and metallization techniques for n-type monocrystalline silicon solar cells. Solar Energy Sustain. Dev. **13**(2), 151–173 (2024). https://doi.org/10.51646/jsesd.v13i2.185
4. H. Belkhanchi, Y. Ziat, M. Hammi, C. Laghlimi, A. Moutcine, A. Benyounes, F. Kzaiber, Nitrogen doped carbon nanotubes grafted TiO_2 rutile nanofilms: promising material for dye sensitized solar cell application. Optik **229**, 166234 (2021). https://doi.org/10.1016/j.ijleo.2020.166234
5. L.A. Rtemi, W. El-Osta, A. Attaiep, Hybrid system modeling for renewable energy sources. Solar Energy Sustain. Dev. **12**(1), 13–28 (2023)
6. M.G.M. Almihat, M.T.E. Kahn, Design and implementation of Hybrid renewable energy (PV/Wind/Diesel/Battery) Microgrids for rural areas. Solar Energy Sustain. Dev. **12**(1), 71–95 (2023)
7. A. Koufi, Y. Ziat, H. Belkhanchi, M. Miri, N. Lakouari, F.Z. Baghli, A computational study of the structural and thermal conduct of MgCrH3 and MgFeH3 perovskite-type hydrides: FP-LAPW and BoltzTraP insight., E3S Web of onferences. EDP Sci. **582**, 02003 (2024). https://doi.org/10.1051/e3sconf/202458202003
8. R. Foster, M. Ghassemi, A. Cota, *Solar Energy: Renewable Energy and the Environment* (CRC Press, 2009)
9. M. Aljuboori, M. Oglah, A. Hasan, Enhancing photoconversion efficiency by optimization of electron/hole transport interlayers in antimony sulfide solar cell using SCAPS-1D simulation. Solar Energy Sustain. Dev. **13**(1), 97–113 (2024). https://doi.org/10.51646/jsesd.v13i1.175
10. F. Yang, Y. Pan, J. Zhu, Enhanced catalytic activity of noble metal@ borophene/WS2 heterojunction for hydrogen evolution reaction. Appl. Surf. Sci. **680**, 161321 (2025)
11. T. Mambrini, *Caractérisation de Panneaux Solaires Photovoltaïques en Conditions Réelles d'Implantation et en Fonction des Différentes Technologies*. Diss. Paris **11**, (2014)
12. F. Zhang, Y. Mao, T.J. Park, S.S. Wong, Green synthesis and property characterization of single-crystalline perovskite fluoride nanorods. Adv. Funct. Mater. **18**(1), 103112 (2008)
13. H. Mu, F. Hu, R. Wang, J. Jia, S. Xiao, Effects of in-situ annealing on the electroluminescence performance of the Sn-based perovskite light-emitting diodes prepared by thermal evaporation. J. Lumin. **226**, 117493 (2020)
14. Q.G. Du, G. Shen, S. John, Light-trapping in perovskite solar cells. AIP Adv. (2016). https://doi.org/10.1063/1.4953336
15. A.S. Bhalla, R. Guo, R. Roy, The perovskite structure—a review of its role in ceramic science and technology. Mater. Res. Innovations **4**(1), 3–26 (2000)
16. Y. Wang, J. Lv, P. Gao, Y. Ma, Crystal structure prediction via efficient sampling of the potential energy surface. Acc. Chem. Res. **55**(15), 2068–2076 (2022)
17. X.Z. Deng, Q.Q. Zhao, Y.Q. Zhao, M.Q. Cai, Theoretical study on photoelectric properties of lead-free mixed inorganic perovskite RbGe1-xSnxI3. Curr. Appl. Phys. **19**(3), 279–284 (2019)
18. M.M. Shabat, H.J. El-Khozondar, S.A. Nassar, G. Zoppi, Y.F. Nassar, Design and optimization of plasmonic nanoparticles-enhanced perovskite solar cells using the FDTD method. Solar Energy Sustain. Dev. **13**(1), 43–56 (2024). https://doi.org/10.51646/jsesd.v13i1.170
19. M. Karouchi, A. Ejjabli, S. Samine, O. Bajjou, Y. Lachtioui, Enhancing the optoelectronic properties of $TiPbO_3$ perovskite through lanthanum doping: an insightful investigation. Solar Energy Sustain. Dev. (2024). https://doi.org/10.51646/jsesd.v14iSI_MSMS2E.397
20. A. Laassouli, L. Moulaoui, A. Najim, H. Errahoui, K. Rahmani, Y. Lachtioui, O.B.O. Bajjou, Phosphorus doping effects on the optoelectronic properties of $K_2AgAsBr_6$ double perovskites for photovoltaic applications. Solar Energy Sustain. Dev. (2024). https://doi.org/10.51646/jsesd.v14iSI_MSMS2E.407
21. A. Koufi, Y. Ziat, H. Belkhanchi, Study of the gravimetric, electronic and thermoelectric properties of XAlH3 (X= Be, Na, K) as hydrogen storage perovskite using DFT and the BoltzTrap software package. Solar Energy Sustain. Dev. (2024). https://doi.org/10.51646/jsesd.v14iSI_MSMS2E.403
22. A. Bouzaid, Y. Ziat, H. Belkhanchi, H. Hamdani, A. Koufi, M. Miri et al., Ab initio study of the structural, electronic, and optical properties of $MgTiO_3$ perovskite materials doped with N and P. E3S Web of Conferences. EDP Sci. **582**, 02006 (2024). https://doi.org/10.1051/e3sconf/202458202006
23. A. Bouzaid, Y. Ziat, H. Belkhanchi, Prediction the effect of (S, Se, Te) doped $MgTiO_3$ on optoelectronic, catalytic, and pH conduct as promised candidate photovoltaic device: Ab initio framework. Int. J. Hydrogen Energy **100**, 20–32 (2025). https://doi.org/10.1016/j.ijhydene.2024.12.284
24. S. Mehmood, Z. Ali, Z. Hashmi, S. Khan, Structural, optoelectronic and elastic properties of quaternary perovskites CaPd3B4O 1 2 (B= Ti, V). Int. J. Mod. Phys. B **33**(19), 1950212 (2019)
25. H.M.T. Farid, A. Mera, T.I. Al-Muhimeed, A.A. AlObaid, H. Albalawi, H.H. Hegazy et al., Optoelectronic and thermoelectric properties of A3AsN (A= Mg, Ca, Sr and Ba) in cubic and orthorhombic phase. J. Mater. Res. Technol. **13**, 1485–1495 (2021)
26. S.A. Khan, H.U. Khan, S. Mehmood, Z. Ali, Structural, electronic, optical and thermoelectric properties in the phases of $AgTaO_3$. Mater. Sci. Semicond. Process. **122**, 105467 (2021)
27. S. Idrissi, S. Ziti, H. Labrim, L. Bahmad, Band gaps of the solar perovskites photovoltaic $CsXCl_3$ (X= Sn, Pb or Ge). Mater. Sci. Semicond. Process. **122**, 105484 (2021)
28. M. Miri, Y. Ziat, H. Belkhanchi, Y.A. El Kadi, The effect of pressure on the structural, optoelectronic and mechanical conduct of the X ZnF_3 (X= Na, K and Rb) perovskite: first-principles study. Int. J. Modern Phys. B. (2024). https://doi.org/10.1142/S0217979225500961
29. M.S. Alam, M. Saiduzzaman, A. Biswas, T. Ahmed, A. Sultana, K.M. Hossain, Tuning band gap and enhancing optical functions of $AGeF_3$ (A= K, Rb) under pressure for improved optoelectronic applications. Sci. Rep. **12**(1), 8663 (2022)

30. M.M.H. Babu, T. Saha, J. Podder, P. Roy, A. Barik, E. Haque, Electronic structure transition of cubic CsSnCl3 under pressure: effect of rPBE and PBEsol functionals and GW method. Heliyon **7**(8), e07796 (2021)
31. T.H. Fischer, J. Almlof, General methods for geometry and wave function optimization. J. Phys. Chem. **96**(24), 9768–9774 (1992)
32. P. Blaha, K. Schwarz, F. Tran, R. Laskowski, G.K. Madsen, L.D. Marks, WIEN2k: an APW+lo program for calculating the properties of solids. J. Chem. Phys. **152**, 074101 (2020). https://doi.org/10.1063/1.5143061
33. F.F. Alharbi, S. Mehmood, Z. Ali, S.R. Khan, M. Khan, H. Alqurashi et al., Structure, electronic and magneto-elastic properties of rare earth nitrides Ln3NIn (Ln= Nd, Pm, Sm, Eu, Gd, Tb) anti-perovskites. Physica B: Condens. Matter **695**, 416544 (2024)
34. Z.M. Elqahtani, S. Aman, S. Mehmood, Z. Ali, A. Hussanan, N. Ahmad et al., n-Type narrow band gap A3InAs3 (A= Sr and Eu) Zintl phase semiconductors for optoelectronic and thermoelectric applications. J. Taibah Univ. Sci. **16**(1), 660–669 (2022)
35. T.A. Taha, S. Mehmood, Z. Ali, S. Khan, S. Aman, H.M.T. Farid et al., Structure, magnetic, opto-electronic and thermoelectric properties of A3In2As4 and A5In2As6 (A= Sr and Eu) Zintl phase compounds. J. Alloys Compd. **938**, 168614 (2023)
36. N. Alwadai, S. Mehmood, Z. Ali, M.S. Al-Buriahi, S. Alomairy, R.Y. Khosa et al., Structural, electronic, elastic and magnetic properties of Ln3QIn (Ln= Ce, Pr and Nd; Q= C and N) anti-perovskites. J. Electron. Mater. **51**(6), 2819–2827 (2022)
37. H.A. Alburaih, S. Aman, S. Mehmood, Z. Ali, S.R. Ejaz, R.Y. Khosa et al., First principle study of opto-electronic and thermoelectric properties of Zintl Phase XIn2Z2 (X= Ca, Sr and Z= As, Sb). Appl. Phys. A **128**(5), 451 (2022)
38. W. Kohn, L.J. Sham, Self-consistent equations including exchange and correlation effects. Phys. Rev. **140**(4A), A1133–A1138 (1965)
39. J.P. Perdew, K. Burke, M. Ernzerhof, Generalized gradient approximation made simple. Phys. Rev. Lett. **77**, 3865 (1996). https://doi.org/10.1103/PhysRevLett.77.3865
40. W. Kohn, Nobel Lecture: electronic structure of matter—wave functions and ensity functionals. Rev. Mod. Phys. **71**, 1253 (1999). https://doi.org/10.1103/RevModPhys.71.1253
41. R.W.G. Wyckoff, *Crystal Structures*, vol. 1, 2nd edn. (John Wiley & Sons, Hoboken, 1963)
42. V.G. Tyuterev, N. Vast, Murnaghan's equation of state for the electronic ground state energy. Comput. Mater. Sci. **38**(2), 350–353 (2006). https://doi.org/10.1016/j.commatsci.2005.08.012
43. C.A. Perottoni, A.S. Pereira, J.A.H. Da Jornada, Periodic Hartree-Fock linear combination of crystalline orbitals calculation of the structure, equation of state and elastic properties of titanium diboride. J. Phys. Condens. Matter **12**(32), 7205 (2000)
44. I.N. Frantsevich, F.F. Voronov, S.A. Bokuta, *Handbook of Elastic Constants and Elastic Moduli of Metals and Nonmetals* (Naukova Dumka, Kiev, 1983)
45. M. Husain, N. Rahman, M. Amami, T. Zaman, M. Sohail, R. Khan et al., Predicting structural, optoelectronic and mechanical properties of germanium based AGeF3 (A= Ga and In) halides perovskites using the DFT computational approach. Opt. Quantum Electron. **55**(6), 536 (2023)
46. S.H. Rabbi, T.I. Asif, M.I. Ahmed, M. Saiduzzaman, M. Islam, Unveiling the pressure-driven modulations in $AGeF_3$ (A= Na, Tl) cubic perovskite halides for enhanced optoelectronic performance. Comput. Condens. Matter **38**, e00887 (2024)
47. T. Sato, S. Takagi, S. Deledda, B.C. Hauback, S.I. Orimo, Extending the applicability of the Goldschmidt tolerance factor to arbitrary ionic compounds. Sci. Rep. **6**(1), 23592 (2016)
48. Y. Pan, New insight into the structural, mechanical and thermodynamic properties of Mo2C MXene as the ultra-high temperature ceramics. Mater. Today Chem. **42**, 102449 (2024)
49. Y. Pan, F. Yang, Structural, hydrogen storage capacity, electronic and optical properties of Li-NH hydrogen storage materials from first-principles investigation. J. Energy Storage **87**, 111492 (2024)
50. Y. Pan, X. Zhang, Theoretical predict the structure, elastic anisotropy and thermodynamic properties of Al5W in Al-rich region. J. Market. Res. **24**, 1792–1801 (2023)
51. Y. Pan, Z. Yang, H. Zhang, Exploring the structural, hydrogen storage capacity, electronic and optical properties of H-rich AlHx (x= 4, 5 and 6) hydrogen storage materials: a first-principles study. Int. J. Hydrogen Energy **82**, 1308–1313 (2024)
52. Y. Pan, The influence of Ag and Cu on the electronic and optical properties of ZrO from first-principles calculations. Mater. Sci. Semicond. Process. **135**, 106084 (2021)
53. Y. Pan, Influence of N-vacancy on the electronic and optical properties of bulk GaN from first-principles investigations. Int. J. Energy Res. **45**(10), 15512–15520 (2021)
54. A.A. Emery, C. Wolverton, High-throughput DFT calculations of formation energy, stability and oxygen vacancy formation energy of ABO3 perovskites. Sci. Data **4**(1), 1–10 (2017)
55. F. Mouhat, F.X. Coudert, Necessary and sufficient elastic stability conditions in various crystal systems. Phys. Rev. B **90**(22), 224104 (2014)
56. J. Wang, Y. Zhou, Dependence of elastic stiffness on electronic band structure of nanolaminate M 2 AlC (M= Ti, V, Nb, and Cr) ceramics. Phys. Rev. B Condens. Matter Mater. Phys. **69**(21), 214111 (2004)
57. M. Born, *On the stability of crystal lattices. I. In Mathematical Proceedings of the Cambridge Philosophical Society*, vol. 36, No. 2 (Cambridge University Press, 1940), pp.160–172
58. Y.O. Ciftci, M. Evecen, First principle study of structural, electronic, mechanical, dynamic and optical properties of half-Heusler compound LiScSi under pressure. Phase Transit. **91**, 1206–1222 (2018)
59. F. Herman, Theoretical investigation of the electronic energy band structure of solids. Rev. Mod. Phys. **30**(1), 102 (1958)

60. H. Bouafia, S. Hiadsi, B. Abidri, A. Akriche, L. Ghalouci, B. Sahli, Structural, elastic, electronic and thermodynamic properties of $KTaO_3$ and $NaTaO_3$: Ab initio investigations. Comput. Mater. Sci. **75**, 1–8 (2013). https://doi.org/10.1016/j.commatsci.2013.03.030
61. A.M. Shawahni, M.S. Abu-Jafar, R.T. Jaradat, T. Ouahrani, R. Khenata, A.A. Mousa, K.F. Ilaiwi, Structural, elastic, electronic and optical properties of SrTMO3 (TM= Rh, Zr) compounds: insights from FP-LAPW study. Materials **11**(10), 2057 (2018). https://doi.org/10.3390/ma11102057
62. R. Hill, The elastic behaviour of a crystalline aggregate. Proc. Phys. Soc. Sect. A **65**(5), 349–354 (1952). https://doi.org/10.1088/0370-1298/65/5/307
63. A. Reuss, Berechnung der fließgrenze von mischkristallen auf grund der plastizitätsbedingung für einkristalle. Z. Angew. Math. Mech. **9**, 49–58 (1929)
64. W. Voigt, *Lehrbuch der Kristallphysik (mit Ausschluss der Kristalloptik)* (B.G. Teubner, Berlin, 1910)
65. S.F. Pugh, XCII. Relations between the elastic moduli and the plastic properties of polycrystalline pure metals. Lond. Edinburgh Dublin Philos. Mag. J. Sci. **45**(367), 823–843 (1954). https://doi.org/10.1080/14786440808520496
66. G. Wang, Y. Jiang, Z. Li, X. Chong, J. Feng, Balance between strength and ductility of dilute Fe2B by high-throughput first-principles calculations. Ceram. Int. **47**(4), 4758–4768 (2021). https://doi.org/10.1016/j.ceramint.2020.10.045
67. H. Fu, D. Li, F. Peng, T. Gao, X. Cheng, Ab initio calculations of elastic constants and thermodynamic properties of NiAl under high pressures. Comput. Mater. Sci. **44**(2), 774–778 (2008)
68. J. Zhu, Y. Pan, Tunability of the electronic structure of GaN third generation semiconductor for enhanced band gap: the influence of B concentration. Mater. Sci. Eng. B **308**, 117554 (2024)
69. Y. Pan, Prediction of the structural, mechanical, and physical properties of GaC: as a potential third-generation semiconductor material. Inorg. Chem. **63**(18), 8264–8272 (2024)
70. A.P. Nayak, S. Bhattacharyya, J. Zhu, J. Liu, X. Wu, T. Pandey et al., Pressure-induced semiconducting to metallic transition in multilayered molybdenum disulphide. Nat. Commun. **5**(1), 1–9 (2014)
71. J. Zhang, Y. Chen, S. Chen, J. Hou, R. Song, Z.F. Shi, Electronic structure, mechanical, optical and thermodynamic properties of cubic perovskite InBeF3 with pressure effects: first-principles calculations. Results Phys. **50**, 106590 (2023)
72. S. Mehmood, Z. Ali, I. Khan, I. Ahmad, Effects of A-site cation on the physical properties of quaternary perovskites AMn3V4O12 (A= Ca, Ce and Sm). Mater. Chem. Phys. **254**, 123229 (2020)
73. A. Nazir, E.A. Khera, M. Manzoor, B.A. Al-Asbahi, Y.A. Kumar, R. Sharma, A density functional theory study of the structural, mechanical, optoelectronics and thermoelectric properties of InGeX3 (X= F, Cl) perovskites. Polyhedron **257**, 117009 (2024)
74. M. Radjai, A. Bouhemadou, & D. Maouche, Structural, elastic, electronic and optical properties of the half-Heusler ScPtSb and YPtSb compounds under pressure. arXiv preprint arXiv:2112.09940 (2021)
75. S. Al Azar, I. Al-Zoubi, A.A. Mousa, R.S. Masharfe, E.K. Jaradat, Investigation of electronic, optical and thermoelectric properties of perovskite BaTMO3 (TM= Zr, Hf): first principles calculations. J. Alloy. Compd. **887**, 161361 (2021)
76. T.V. Vu, H.D. Tong, D.P. Tran, N.T. Binh, C.V. Nguyen, H.V. Phuc et al., Electronic and optical properties of Janus ZrSSe by density functional theory. RSC Adv. **9**(70), 41058–41065 (2019)
77. Y. Ziat, A. Abbassi, A. Slassi, M. Hammi, A.A. Raiss, O.E. Rhazouani et al., First-principles investigation of the electronic and optical properties of Al-doped FeS_2 pyrite for photovoltaic applications. Opt. Quantum Electron. **48**, 1–8 (2016)
78. Y. Ziat, H. Belkhanchi, Z. Zarhri, DFT analysis of structural, electrical, and optical properties of S, Si, and F-Doped GeO_2 Rutile: implications for UV-transparent conductors and photodetection. Solar Energy Sustain. Dev. **14**(1), 74–89 (2025). https://doi.org/10.5164/jsesd.v14i1.232
79. A. Bianconi, S.B.M. Hagström, R.Z. Bachrach, Photoemission studies of graphite, high-energy conduction-band and valence-band states using soft-x-ray synchrotron radiation, excitation. Phys. Rev. B **16**(12), 5543 (1977)
80. L.H. Gray, The absorption of penetrating radiation. Proc. R Soc. Lond. Ser. A Contain. Paper Math. Phys. Character **122**(790), 647–668 (1929)
81. S. Hasegawa, Reflection high-energy electron diffraction. Characteriz. Mater. **97**, 1925–1938 (2012)
82. S. Mehmood, N. Khan, Z. Ali, I. Khan, S.A. Alsalhi, Photovoltaic properties of halide perovskites for solar cell application with efficiency greater than 18%. RSC Adv. **14**(42), 30606–30617 (2024)
83. H.A. Alsalmah, S. Mehmood, First-principles calculation to investigate structural and opto-electronic properties of transition base halide perovskite oxides for solar cell applications. Sol. Energy **273**, 112498 (2024)